ORIGINAL ARTICLE

Modeling heterogeneous plasticity of human bone for orthopedic applications using 3D biomechanics

Muhammad Hamza Arshad Khan[1], Zartasha Mustansar[2*], Sumair Naseem Qureshi[3]

Biomedica - Official Journal of University of Health Sciences, Lahore, Pakistan
Volume 41(3):89-96
https://doi.org/10.24911/BioMedica/5-2226

OPEN ACCESS

This is an open access article distributed in accordance with the Creative Commons Attribution (CC BY 4.0) license: https://creativecommons.org/licenses/by/4.0/ which permits any use, Share — copy and redistribute the material in any medium or format, Adapt — remix, transform, and build upon the material for any purpose, as long as the authors and the original source are properly cited. © The Author(s) 2025

ABSTRACT

Background and Objective: Modeling the density-based heterogeneous nature of bones, specifically their plasticity, poses a significant challenge in computational modeling. Although the cortical bone is brittle and has very little plastic deformation, the trabecular bone deforms plastically through repeated loading cycles. Most computational models take into account the density-based heterogeneity of the elastic region; however, this research presents an approach to include heterogeneity in the plastic region of a Finite Element (FE) model using Ansys scripting.

Methods: A FE model of the distal femur from a Computerized Tomography (CT) scan has been created, and the material properties have been incorporated using an Ansys script for both elastic and plastic deformation. Heterogeneity in the plastic region has been included by using TB, Plas, Material ID, 1, Plasticity Material Model Ansys function.

Results: A displacement of 0.1 mm applied at the distal end of the femur generated stresses exceeding the yield strength, resulting in plastic deformation. The diaphysis, which is made up mostly of cortical bone, has shown no plastic deformation, whereas the epiphysis, with trabecular bone, has shown plasticity.

Conclusion: This research makes significant improvements in FE modeling by taking into consideration the inhomogeneous and plastic nature of bone. This research holds serious importance for the development of implants, prediction of fracture, and biomechanics research.

Keywords: Bone remodeling, CT scan, image segments, Finite element (FE), plasticity.

Received: 23 March 2025 **Revised:** 17 July 2025 **Accepted:** 23 August 2025

Correspondence to: Zartasha Mustansar
*SINES National University of Sciences and Technology H12 Islamabad.
Email: zmustansar@sines.nust.edu.pk
Full list of author information is available at the end of the article.

Introduction

Bone is an anisotropic material where mechanical properties of bone depend on bone orientation. Such mechanical properties depend on collagen fibers and hydroxyapatite crystals orientation in the bone, which influence the stiffness, strength, and toughness of bone[1]. Bone modulus, or bone stiffness, depends not only on its density but also on the bone structure.

Bone consists of two types of tissue: cortical bone and trabecular bone. In contrast to cortical bone, which is solid, hard, and brittle, trabecular bone is porous, spongy, and elastic[2]. The special structure of bones allows them to withstand mechanical stresses. Anisotropy of bone structure allows effective use of the load-bearing properties of bone in certain directions while reducing its ability to bear loads in other directions.[3]

Among all bones in the human body, the femur is the biggest and the most solid bone, which bears weight and absorbs shocks. The bone is subjected to great mechanical stress during such activities as walking, running, and jumping. Mechanical stresses exerted on the femur differ greatly depending on particular physical activity and can be minimal or extremely high. These repetitive high loads create stress concentrations, which over time can lead to micro-damage accumulation, reduced bone longevity, and potential failure[4].

The mechanical response of bones under varying loading conditions is also different, having a greater capacity to withstand compressive loads than tensile, bending, or torsional forces. Since the cortical bone is brittle in nature, it does not show much plastic deformation under load. In contrast, trabecular bone, being porous in nature, shows substantial plastic deformation under load[5]. Current

experiments have confirmed that trabecular bone is softer in nature, which has lesser stiffness and yield strength as compared to cortical bone, which still behaves brittle at the same load conditions[6]. Moreover, the rate of strain is also important in understanding the mechanics of bone failure. Under high strain rates, for example, when bones experience an impact or trauma, bones generally fail in a brittle fashion. But under low strain rates, which are experienced in daily life activities, bones show some ductility, which allows them to deform before failing[7].

For modeling the anisotropic behavior of the bone, new methods have been created based on micro-CT scans. This process allows the acquisition of bone geometry and further calculation of the elastic modulus according to the correlation between Hounsfield units (HUs) and bone density[3,8]. Out of all the existing methods, this one provides the most accurate results for material properties in FE models. Other approaches may include considering the whole bone as an isotropic material and assigning one modulus for both parts of the bone (cortical and trabecular), as well as the application of the orthotropic model (when the material properties are assigned in three mutually perpendicular directions)[9]. Considering the high anisotropy of bone, the most accurate way to apply material properties in FE models is through HU data received from CT scans. Such a method has been used widely in the literature for evaluation of bone mechanical strength in various anatomical locations[10]. In addition, recent research using CT-based finite element (FE) modeling has shown that density-mapped models can accurately predict how real bone behaves under loading, especially in trabecular regions [11]**.** However, previous studies have primarily focused on the elastic behavior of bone, neglecting the plasticity aspect.[8-11]

For any structural materials, the deformation process follows the linear elastic phase, whereby the deformation of the material will be restored when the load is released. Once the yield strength is exceeded, the deformation becomes plastic, and there are permanent changes in the structure of the material[5]. Multiscale modeling investigations have recently shown that bone is also similar to such materials in that post-yield behavior occurs in which plastic flow appears at the level of fibril arrays and leads to a complex response of the material to cyclic loading.[12] Based on the aforementioned studies, recent CT-based FE methods incorporate coupled damage-plasticity approaches to mimic the nonlinear deformation and localization of failure of bones. However, despite the advancements in the field, most FE analyses of density-based heterogeneous bone still focus on elasticity rather than plasticity.[13,14]

The current study attempts to address this deficiency by introducing plasticity into HU-based material characterization. Through FE modeling of materials outside the elastic phase, this study hopes to achieve a comprehensive insight into bone mechanics.

Methods

Retrospective imaging data obtained from computed tomography (CT) were used in this study; however, these were owned by the corresponding author of the study. The imaging data were originally collected during normal clinical

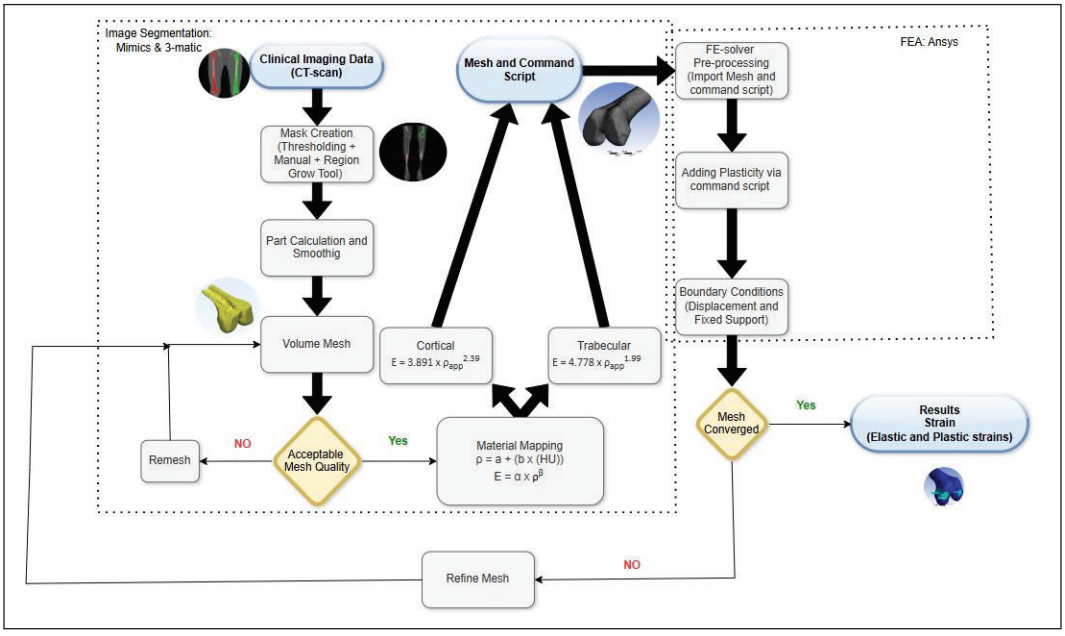


Figure 1. *Flowchart of non-invasive biomechanical inspection of bone*

practice at Shifa International Hospital, Islamabad. These were later analyzed in a computational biomechanics study. Prior to their analysis, all imaging data were completely anonymized to ensure no personal data remained.

Since the data consisted only of anonymized clinical imaging data of the corresponding author and no human participants were recruited or involved in this study, this study does not represent a human participant experiment. Written consent was obtained from the corresponding author to use their anonymized imaging data in this study.

In compliance with institutional guidelines on conducting studies involving retrospective and self-provided anonymized clinical data, the study was carried out as a computational modeling experiment without any human or animal experiment. The stepwise non-invasive biomechanical inspection method has been highlighted in Figure 1.

A CT scan dataset de-identified for one human femur (*n* = 1), was obtained from a collaborating hospital. CT scans were acquired on a Toshiba Aquilion One 640-slice CT scanner with a 100 kW generator. The CT volume comprised 640 slices with a slice thickness of 1 mm and in-plane pixel spacing of 0.856 mm. All of the data were anonymized before any further processing to protect the confidentiality of the patient.

The CT scans were imported into Materialize Mimics software (version 21.0), and bone tissue was segmented from the CT scans using a global threshold value ranging from 226 to 3071 HU. After the initial thresholding, region growing, morphological processing, and manual editing were done to clean up the mask and remove unwanted regions, including distal femoral sections, foot bones, and image artifacts. After segmentation, the mask was exported to Materialize 3-matic software (version 21.0) to perform surface reconstruction and smoothing.

Material properties were assigned based on HU–derived density correlations. Recent studies have shown that HU–based material mapping provides a more realistic way to assign varying bone densities in FE models, helping improve accuracy in predicting real mechanical behavior[15]. The relationship between HU and apparent density (ρ) followed a linear correlation given by:

$$\rho = a + (b \times H) \quad (1)$$

where 'a' and 'b' are attenuation coefficients. In this study, the equation proposed by Buenger (16) was adopted:

$$\rho = 17.8 + (0.7 \times H)\ kg/m^3 \quad (2)$$

The conversion from HU to apparent bone density was performed using the published relationship proposed by Buenger et al.[16] This equation was adopted from the literature and was not recalibrated using a scanner-specific calibration phantom for the CT system and acquisition protocol employed in this study. The computed densities were then converted to Young's modulus (E) using power-law relationships derived from the literature, expressed as:

$$E = \alpha \times \rho^{\beta}\ Pa \quad (3)$$

Based on previous studies, 20 distinct material groups were defined to represent both cortical and trabecular regions (Table 1). Material IDs 1–2 corresponded to void or very low-density regions, 3–12 represented trabecular bone (150–600 HU), and 13–22 represented cortical bone (600–2000 HU).

The modulus equation for the trabecular region was proposed by Linde and colleagues, [17] whereas the cortical region equation was proposed by Schneider and Snyder[18]. The transition point between cortical and trabecular bone was set at 600 HU based on findings in the literature that support this threshold as an effective delineation between the two regions[19]. The material mapping methodology involved selecting elements of the volume mesh, identifying their coordinates relative to the clinical image (CT scan), determining the average HU value at each element's location, and assigning appropriate material properties based on trabecular or cortical classification. By integrating plasticity modeling into this HU-based material mapping, this study aims to enhance FE analysis accuracy, ultimately providing deeper insights into bone mechanics and improving applications in orthopedic research, implant design, and injury prevention strategies.

A consistent SI unit system was used for both the material mapping and FE simulation process. Bone density

Table 1. *Classification of femoral bone material types based on Hounsfield unit (HU) ranges and corresponding density–elasticity relationships used for material property assignment in finite element modelling.*

Sr. No.	Material IDs	Bone type	HU value	Equation
1	1	Void	Negative HU values	NIL
2	2	Void	Very low HU values	NIL
3	3–12	Trabecular	150–600	$E = 4.778 \times \rho^{1.99}$ App
4	13–22	Cortical	600–2000	$E = 3.891 \times \rho^{2.39}$ App

ρ, determined from CT HU values, is given in kilograms per cubic meter (kg/m³). The empirical power laws for Young's modulus E, determined from the data of Linde[17] and Schneider and Snyder[18], were calculated first in Pa before conversion into MPa for use in the ANSYS APDL solver.

For the FE simulation, all parameters involving stress, such as yield stress σy and tangent modulus Et, were given in MPa to conform to the consistent ANSYS mechanical unit system. This means that the solver was using a consistent unit system where length is in mm, force is in N, stress is in MPa, and density is in kg/m³.

After assigning the materials, the FE mesh developed in Mimics was brought to Ansys Mechanical 2023 for simulation. Mesh generation was carried out using two main parts: the .cbdb file, which has the geometric information of the mesh, and the command script, which has the material properties assigned to the different materials. By default, this script takes care of only the elastic nature of the bone; hence, changes have been done to accommodate the plastic behavior of the bones by incorporating the yield stress and plastic deformation depending on the local density.

Femur geometry has been meshed using four-node linear tetrahedral elements, producing 2,007,690 elements in total. The mesh had an average edge length of 0.594 mm, with the minimum and maximum edge lengths being 3.15 × 10^{-3} mm and 1.96 mm, respectively. The quality of the mesh had an average value of 0.745, and about 95% of the elements have a quality value greater than 0.5 and close to 1. The average element aspect ratio is 2.42, meaning that the elements are well shaped for numerical evaluation. The proximal diaphysis part of the femur is completely restrained. A compressive displacement of 0.1 mm was specified at the distal femoral epiphysis in order to simulate physiological loading conditions. No interaction was specified between any of the surfaces in the model. The mechanical response of bone material was characterized using an isotropic bilinear plasticity model, where the yield strength is a function of the bone material density.

The simulation was performed for quasi-static loading. Geometric non-linearity (large deflections) was enabled in the analysis. This setting made the simulation more accurate, as it better simulated the real-life behavior of bone material under compressive loading.

To define plasticity in the FE model, the following script was utilized:

TB, Plas, Material ID, 1, Plasticity Material Model
TBDATA, 1, Yield Strength, Tangent Modulus

However, the script needs to be individually run for each material ID that characterizes the elastic part of the bone (either cortical or trabecular). In the current analysis, 20 material IDs have been used for modeling the bone; hence, a plasticity model had to be defined for each of these 20 materials. But, the input parameters for the script depend upon the type of bone, which in turn refers to whether it is cortical or trabecular. (Table 2)

For example, the script was modified as per the following details for specific material IDs:

Each line in the script is dedicated to one material ID, and the tangent modulus was varied in accordance with Young's modulus for the material ID concerned. The values of the yield strength for both trabecular and cortical bone subjected to compressive loading are as per Havaldar et al.[20,] wherein the mechanical properties of the bones of males aged below 30 years have been studied. Tangent modulus, which denotes the slope of the stress–strain curve in the plastic region, has been calculated using the procedure by Niebur[21].

Specifically, for bone tissue, the tangent modulus is estimated to be 5% of the Young's modulus in the elastic region (Figure 2). This linear approximation simplifies the non-linear behavior observed during plastic deformation.

Yield strength was not considered as a continuous function of density/HU. In contrast, there were two values of yield strength for two major types of bones included in the bone structure: trabecular and cortical. The material ID of trabecular bone had its own value of the yield strength,

Table 2. *Bone type and corresponding script*

Bone Type	Script
Trabecular (3rd material)	TB, Plas, 3, 1, BISO TBDATA, 1, 5.12, 4409
Cortical (13th material)	TB, Plas, 13, 1, BISO TBDATA, 1, 160, 539075

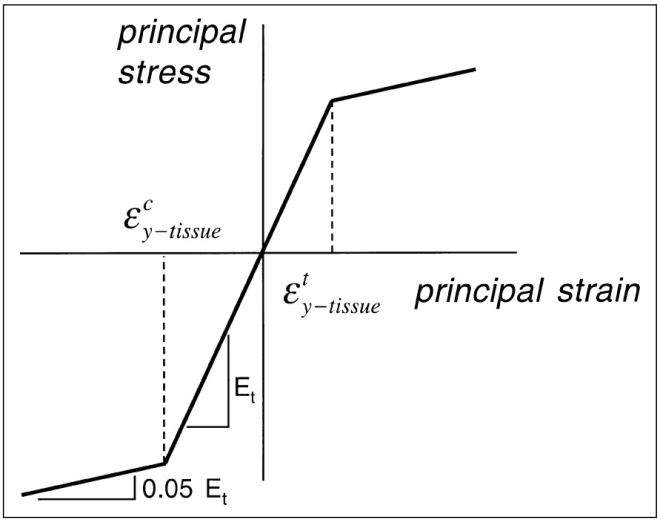


Figure 2. *Youngs modulus approximation in plastic region*

while the material ID of cortical bone was characterized by another, greater value of the yield strength.

The tangent modulus for the bilinear plasticity model was proportional to the Young's modulus of each material ID. As a consequence, despite the fact that there were only two constant values of yield strength, there were variations in the tangent modulus among the 20 material IDs because of the dependence of the Young's modulus on density.

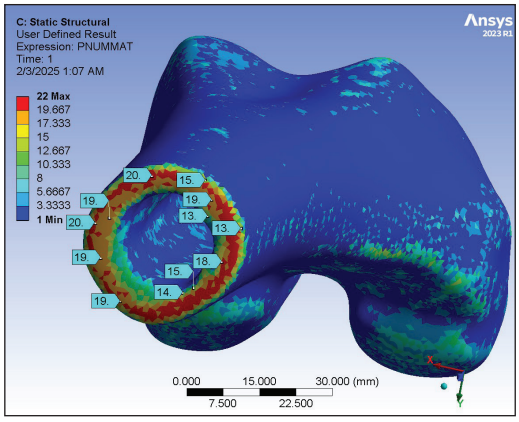
The use of the bilinear isotropic plasticity model for all material IDs leads to heterogeneous behavior of the bone FE model in both elastic and plastic phases. While the current work uses the bilinear isotropic plasticity model, it is possible to consider other, more complicated plasticity models such as multi-linear isotropic plasticity or kinematic plasticity in future studies.

Results

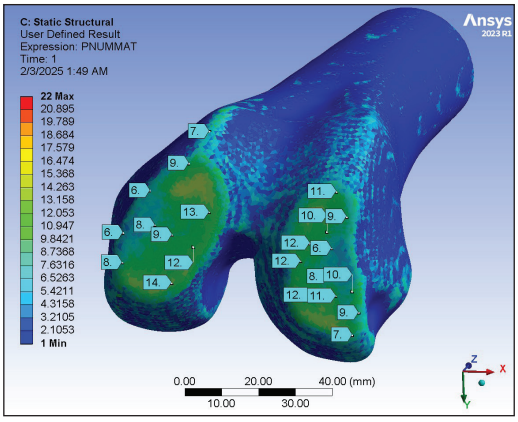
In order to quantitatively evaluate the realism of HU-based material mapping, material ID distribution in the FE mesh was analyzed. In the resulting mapped model, mainly trabecular bone elements (material IDs 3–12) have been found in the epiphyseal regions, whereas dense cortical bone elements (material IDs 13–22) were identified in the diaphyseal region; see Figure 3.

As follows from the material mapping based on the material assignment for individual elements, approximately ~60%–65% of the elements are trabecular bone elements, while ~30%–35% correspond to cortical bone elements, with the rest being low-density elements of marrow or voids. The volume distribution was similar, which reflects the fact that there is more volume of trabecular bone in epiphyseal regions and dense cortical bone in the shaft. Thus, the obtained material distribution (Figure 4) shows the smooth transition from low-density trabecular tissue to dense cortical bone, which agrees well with the knowledge about femur anatomy and results of other FE studies based on CT data. Therefore, it is clear that the HU-based material mapping resulted in realistic tissue heterogeneity.

Mesh generation was done using tetrahedron elements, a total of 2,007,690 elements. A displacement of 0.1 mm was applied to the distal femoral epiphysis so that we could evaluate the strains induced in both cortical and trabecular portions. The highest elastic strain value recorded was 517



(a) Cortical Bone Region



(b) Trabecular Bone Region

Figure 3. *Material IDs for cortical and trabecular bone*

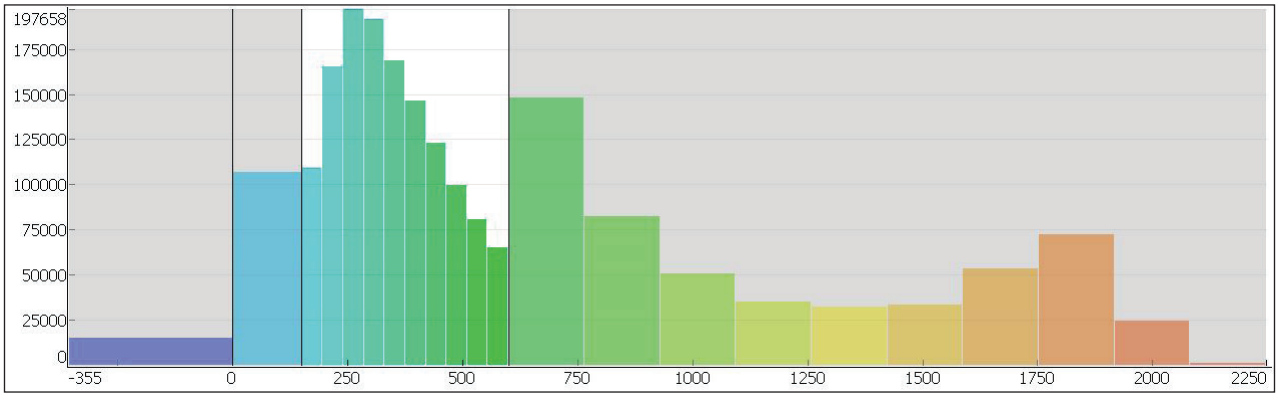
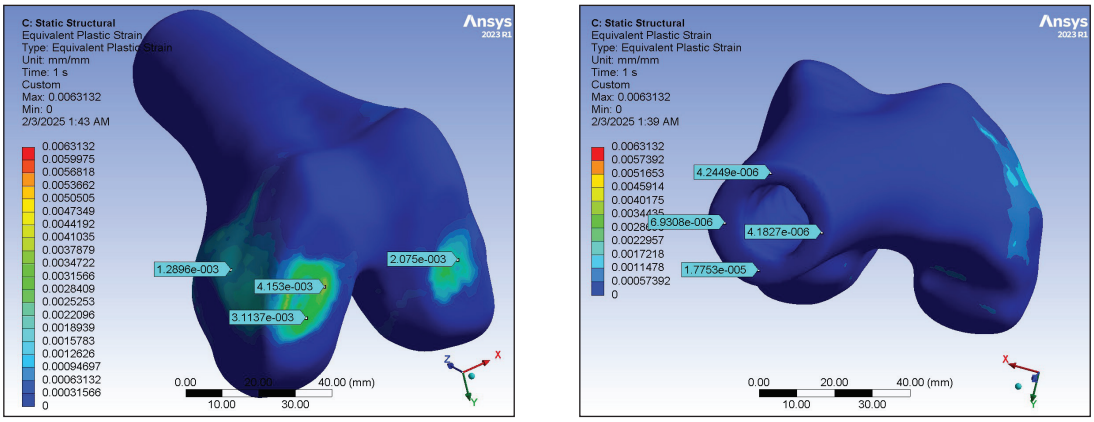


Figure 4. *Element numbers per material classification*



(a) Epiphysis **(b) Diaphysis**

Figure 5. *Plastic strains*

(με), while the average elastic strain value was 36.8 (με). More importantly, it should be noted that the induced displacement deformed the bone to the extent of going beyond its yield point. (Fig-5)

Discussion

Within the limits of a single femur specimen model (*n* = 1) and simplification of boundary conditions, the current analysis separates the mechanical behavior of cortical and trabecular areas in compression. While diaphyseal cortical bone was primarily in an elastic state, epiphyseal trabecular bone had plastic behavior due to lower stiffness and greater deformability. Cortical bone is stiffer and able to tolerate greater ultimate stresses compared to trabecular bone, but is also more brittle. Trabecular bone in vitro can tolerate strains of up to 30%, while cortical bone is subject to failure at strain levels of 2%[22]. The difference between these two bone tissues could be distinguished by the parameter of porosity; the porosity level of cortical bone is 5–15%, while trabecular bone porosity lies in the range of 40–95%; cortical bone exists in the diaphyseal part of long bones and as a thin layer around the trabecular compartment in metaphyses and epiphyses[23]. The inclusion of a bilinear isotropic plasticity model extended the simulations beyond the elastic region and provided a more realistic representation of post-yield bone behavior. Material mapping based on HU, combined with density-dependent tangent moduli, enabled the capture of localized yielding within trabecular regions while maintaining elastic behavior in cortical bone. Realistic macro-level FE simulations of the mechanical behavior of trabecular bone require a suitable constitutive model that incorporates the mechanical response of bone for complex loading scenarios and includes post-elastic phenomena, such as plasticity (permanent deformations) and damage (permanent stiffness reduction), which bone is likely to experience[24].

Although the loading conditions were simplified and time-dependent or viscoelastic effects were not considered, the observed deformation patterns are consistent with experimental findings reporting progressive yielding in trabecular bone under compression and comparatively brittle behavior in cortical bone. The stress–strain curve for trabecular bone under compression is characteristic of that of other cellular solids, comprising three distinct regimes: a linear elastic region for its initial response, followed by a stress plateau (the plastic region) where stress remains relatively constant along with significant bone deformation corresponding to trabecular bone collapse by elastic buckling, plastic yielding, or brittle crushing[25]. However, the absence of experimental validation limits direct quantitative comparison, and the results should therefore be interpreted as qualitative and comparative rather than predictive.

Despite these limitations, the proposed modeling framework provides valuable insight into spatially heterogeneous bone mechanics and highlights the importance of incorporating plasticity into CT-based FE analyses. Subject-specific FE models of bones from CT data have been proposed to improve fracture risk prediction, since they can take into account the structural determinants of bone strength and the variety of external loads acting on bones[26]. This approach lays a foundation for future work incorporating subject cohorts, physiologically realistic loading, time-dependent material behavior, and experimental validation to support applications in bone–implant mechanics, fracture prediction, and heterogeneous material modeling.

Limitations of the Study

This study has certain limitations that should be acknowledged. The analysis was conducted using a single femur CT dataset, which may restrict the generalizability of the findings. The applied boundary conditions represented

simplified compressive loading and may not fully capture the complex physiological loads experienced by the femur in vivo. Although heterogeneous material mapping was employed, the plasticity model did not account for viscoelastic or time-dependent behavior of bone tissue. Furthermore, due to the non-invasive nature of the work, experimental validation of the simulated results could not be performed

Conclusion

In conclusion, this research reveals the importance of the heterogeneous nature of the bone structure and the necessity to consider its plastic properties while improving the process of FEA for biomechanical purposes. By means of using modern imaging technologies and expanding the area of simulations to the plastic deformation zone, this research presents a broader vision of the processes taking place in bones. The results prove that cortical and trabecular bone structures behave differently during the process of deformation, and the consideration of specific materials for different regions is required. These simulations have not only the potential to increase the accuracy of computer models but also have numerous clinical applications in terms of diagnostics and the creation of implants and therapeutic approaches to bone pathologies. Future studies might include more advanced plasticity models, including multi-linear or kinematic plasticity.

Acknowledgment

The author gratefully acknowledges the support and collaborative research environment of the Biomechanics Laboratory at the National University of Sciences and Technology (NUST), Pakistan. The author also acknowledges the Higher Education Commission (HEC) of Pakistan for financial support of this study.

List of Abbreviations

CT	Computed Tomography
FE	Finite Element
HU	Hounsfield Unit
SI	International System of Units

Conflict of interest

None to declare.

Grant support and financial disclosure

This study was funded by the Higher Education Commission of Pakistan (HEC), under the grant code 16076.

Ethical approval

Ethical approval was obtained from the Institutional Review Board of NUST (Ref. No. 6-2022-ASAB-01/07, dated: 28-06-2024)

Author's contribution

M.H.A.K: Conducted experiments and ran simulations. M.H.A.K also drafted the manuscript from the beginning.
Z.M: Acquired the funding, conceptualized the study, and provided overall supervision and review.
S.N.Q: Reviewed the work and contributed clinical insights
All AUTHORS: Approval and full responsibility for the final version of the manuscript to be published.

Authors' Details

Muhammad Hamza Arshad Khan[1], Zartasha Mustansar[2], Sumair Naseem Qureshi3

1. MS Research Scholar. School of Interdisciplinary Engineering & Science (SINES), National University of Sciences and Technology, Islamabad, Pakistan
2. Professor and Head of Department, School of Interdisciplinary Engineering & Science (SINES), National University of Sciences and Technology, Islamabad, Pakistan
3. Department of Orthopedic Surgery, Shifa College of Medicine and Shifa International Hospital, Islamabad, Pakistan

References

1. Qin Z, Gautieri A, Nair AK, Inbar H, Buehler MJ. Thickness of hydroxyapatite nanocrystal controls mechanical properties of the collagen-hydroxyapatite interface. Langmuir. 2012;28(4):1982–92. https://doi.org/10.1021/la204052a
2. Bhuiyan D, Middleton J, Tannenbaum R. Development of hydroxyapatite-mediated synthesis of collagen-based copolymers for application as bio scaffolds in bone regeneration. MRS Online Proc Libr. 2014;1621:53–8. https://doi.org/10.1557/opl.2014.286
3. Morgan EF, Unnikrisnan GU, Hussein AI. Bone Mechanical Properties in Healthy and Diseased States. Annu Rev Biomed Eng. 2018 Jun 4;20:119–143. https://doi.org/10.1146/annurev-bioeng-062117-121139. PMID: 29865872; PMCID: PMC6053074.
4. Silva CC, Thomazini D, Pinheiro AG, Aranha N, Figueiró SD, Góes JC, et al. Collagen-hydroxyapatite films: Piezoelectric properties. Mater Sci Eng B. 2001;86(3):210–8. https://doi.org/10.1016/S0921-5107(01)00674-2
5. Kazembakhshi S, Luo Y. Constructing anisotropic finite element model of bone from computed tomography (CT). Biomed Mater Eng. 2014;24(6):2619–26. https://doi.org/10.3233/BME-141078
6. Bittner-Frank M, Reisinger AG, Andriotis OG, Pahr DH, Thurner PJ. Cortical and trabecular mechanical properties in the femoral neck vary differently with changes in bone mineral density. JBMR Plus. 2024;8(6). https://doi.org/10.1093/jbmrpl/ziae049
7. Fox S, Stamshevskaya I, Chowdhury S, Catledge S, Stanishevsky A. Mechanical properties of nanoparticle hydroxyapatitelgelatin constructs. Mater Res Soc Symp Proc. 2008;1063(504):58–63. https://doi.org/10.1557/PROC-1063-OO05-04
8. Schwiedrzik JJ, Zysset PK. An anisotropic elastic-viscoplastic damage model for bone tissue. Biomech Model Mechanobiol. 2013;12(2):201–13. https://doi.org/10.1007/s10237-012-0392-9
9. Kenedi PP, Vignoli LL. Bone anisotropy influence - a finite element analysis. XXIV Brazilian Congr Biomed Eng – CBEB 2014. 2014;3(1):798–801.
10. Hosseini HS, Horák M, Zysset PK, Jirásek M. An over-nonlocal implicit gradient-enhanced damage-plastic model for trabecular bone under large compressive strains. Int J Numer Method Biomed Eng. 2015 Nov;31(11). https://doi.org/10.1002/cnm.2728. Epub 2015 Jun 14. PMID: 26033968.;

11. Guha I, Zhang X, Rajapakse CS, Chang G, Saha PK. Finite element analysis of trabecular bone microstructure using CT imaging and continuum mechanical modeling. Med Phys. 2022;49(6):3886–99.
12. Alizadeh E, Omairey S, Zysset P. Investigating the post-yield behavior of mineralized bone fibril arrays using a 3D non-linear finite element unit-cell model. J Mech Behav Biomed Mater. 2023;139:105660. https://doi.org/10.1016/j.jmbbm.2023.105660
13. Soltani Z, Xu M, Radovitzky R, Stadelmann MA, Hackney D, Alkalay RN. CT-based finite element simulating spatial bone damage accumulation predicts metastatic human vertebrae strength and stiffness. Front Bioeng Biotechnol. 2024;12:1424553. https://doi.org/10.3389/fbioe.2024.1424553
14. Sharma N, Sharma S, Sehgal D, Pandey R. Detailed analysis of deformation behavior of plexiform bone using small specimen testing and finite element simulation. In: Pant M, Deep K, Bansal JC, Nagar A, Das KN, editors. Proceedings of the Third International Conference on Soft Computing for Problem Solving (SocProS 2013). Advances in Intelligent Systems and Computing. Vol. 258. New Delhi: Springer; 2014. pp. 479–488. https://doi.org10.1007/978-94-017-9115-1_48.
15. Soodmand I, Becker AK, Sass JO, Jabs C, Kebbach M, Wanke G, et al. Heterogeneous material models for finite element analysis of the human mandible bone – a systematic review. Heliyon. 2024;10(24):e40668. https://doi.org/10.1016/j.heliyon.2024.e40668
16. Buenger F, Eckardt N, Sakr Y, Senft C, Schwarz F. Correlation of bone density values of quantitative computed tomography and Hounsfield units measured in native computed tomography in 902 vertebral bodies. World Neurosurg. 2021;151:e599–e606. https://doi.org/10.1016/j.wneu.2021.04.093.
17. Linde F, Hvid I, Madsen F. The effect of specimen geometry on the mechanical behaviour of trabecular bone specimens. J Biomech. 1992 Apr;25(4):359–68. https://doi.org/10.1016/0021-9290(92)90255-y. PMID: 1583015.
18. Snyder SM, Schneider E. Estimation of mechanical properties of cortical bone by computed tomography. J Orthop Res. 1991 May;9(3):422–31. https://doi.org/10.1002/jor.1100090315. PMID: 2010847.
19. Aamodt A, Kvistad KA, Andersen E, Lund-Larsen J, Eine J, Benum P, Husby OS. Determination of Hounsfield value for CT-based design of custom femoral stems. J Bone Joint Surg Br. 1999 Jan;81(1):143–7. PMID: 10068022.
20. Havaldar R, Pilli SC, Putti BB. Insights into the effects of tensile and compressive loadings on human femur bone. Adv Biomed Res. 2014 Mar 25;3:101. https://doi.org/10.4103/2277-9175.129375. PMID: 24800190; PMCID: PMC4007336.
21. Niebur GL, Feldstein MJ, Yuen JC, Chen TJ, Keaveny TM. High-resolution finite element models with tissue strength asymmetry accurately predict failure of trabecular bone. J Biomech. 2000 Dec;33(12):1575-83. https://doi.org/10.1016/s0021-9290(00)00149-4. PMID: 11006381.
22. Osterhoff G, Morgan EF, Shefelbine SJ, Karim L, McNamara LM, Augat P. Bone mechanical properties and changes with osteoporosis. Injury. 2016 Jun;47 Suppl 2(Suppl 2):S11–20. https://doi.org/10.1016/S0020-1383(16)47003-8. PMID: 27338221; PMCID: PMC4955555.
23. Ibrahim A, Jiang Z, Shirvani K, Dalili A, Abdel Hamid Z. A novel viscoelastic deformation mechanism uncovered during vickers hardness study of bone. J Func Biomater. 2024; 15(4):87. https://https://doi.org/10.3390/jfb15040087
24. Levrero-Florencio F, Pankaj P. Using non-linear homogenization to improve the performance of macroscopic damage models of trabecular bone. Front Physiol. 2018 May 17;9:545. https://doi.org/10.3389/fphys.2018.00545. PMID: 29867581; PMCID: PMC5966630.
25. Limzider N, Rittel D, Shemtov-Yona K. Bone morphology and mechanical behavior: new insights into cortical and trabecular failure under compression. J Mech Behav Biomed Mater. 2026 Jan;173:107214. https://doi.org/10.1016/j.jmbbm.2025.107214. Epub 2025 Sep 26. PMID: 41043218.
26. Grassi L, Schileo E, Taddei F, Zani L, Juszczyk M, Cristofolini L, Viceconti M. Accuracy of finite element predictions in sideways load configurations for the proximal human femur. J Biomech. 2012 Jan 10;45(2):394–9. https://doi.org/10.1016/j.jbiomech.2011.10.019. Epub 2011 Nov 12. PMID: 22079387.